Probody therapeutic design of 89Zr-CX-072 promotes accumulation in PD-L1 expressing tumors compared to normal murine lymphoid tissue

Giesen, Danique; Broer, Linda N; Lub-de Hooge, Marjolijn N; Popova, Irina; Howng, Bruce; Nguyen, Margaret; Vasiljeva, Olga; de Vries, Elisabeth G E; Pool, Martin

Published in:
Clinical Cancer Research

DOI:
10.1158/1078-0432.CCR-19-3137

Document Version
Final author's version (accepted by publisher, after peer review)

Publication date:
2020

Probody therapeutic design of ^{89}Zr-CX-072 promotes accumulation in PD-L1-expressing tumors compared to normal murine lymphoid tissue

Authors

Danique Giesen[1], Linda N. Broer[1], Marjolijn N. Lub-de Hooge[2,3], Irina Popova[4], Bruce Howng[4], Margaret Nguyen[4], Olga Vasiljeva[4]*, Elisabeth G. E. de Vries[1]*, Martin Pool[1]

Affiliations

[1]Department of Medical Oncology, University Medical Center Groningen, University of Groningen, Groningen, the Netherlands;

[2]Department of Clinical Pharmacy and Pharmacology, University Medical Center Groningen, University of Groningen, Groningen, the Netherlands;

[3]Department of Nuclear Medicine and Molecular Imaging, University Medical Center Groningen, University of Groningen, Groningen, the Netherlands;

[4]CytomX Therapeutics Inc., South San Francisco, CA.

Running title

Therapeutic design of anti-PD-L1 Probody CX-072

Corresponding authors

*Olga Vasiljeva, PhD, CytomX Therapeutics Inc., 151 Oyster Point Blvd., South San Francisco, CA 94080, email: ovasiljeva@cytomx.com, phone: (+1)650 515 3912.

*Elisabeth G. E. de Vries, MD, PhD, Department of Medical Oncology, University of Groningen, University Medical Center Groningen, P.O. Box 30.001, 9700 RB Groningen, the Netherlands; e-mail: e.g.e.de.vries@umcg.nl, phone: (+31)50 3612934, fax: (+31)50 3614862.

Disclosure of potential conflicts of interest

A research grant to E. G. E. de Vries was obtained from CytomX Therapeutics and made available to the institution. I. Popova, B. Howng, M. Nguyen and O. Vasiljeva are employees of CytomX Therapeutics, which developed and owns the intellectual property rights pertaining to CX-072. A patent application related to this work has been filed by CytomX Therapeutics.

Translational relevance

Combining immune checkpoint inhibitors improves survival of patients with advanced stages of several tumor types, but can elicit severe immune-related adverse events (irAEs). These irAEs may be caused by immune checkpoint-blockade in healthy tissues and immune checkpoint-inhibiting antibodies with tumor-restricted activity are therefore of interest. Recently, imaging of ^{89}Zr-atezolizumab whole-body distribution in cancer patients showed high uptake in healthy lymphoid tissues, including spleen, lymph nodes and Waldeyer's ring. Our preclinical imaging study in mice reveals anti-PD-L1 Probody therapeutic CX-072 is preferentially activated in tumors, followed by PD-L1-mediated uptake, whereas accumulation in spleen and other PD-L1-expressing peripheral lymphoid tissues is limited. These findings demonstrate CX-072 may reduce anti-PD-L1-mediated toxicities in healthy tissues, thereby potentially expanding its use in combination therapies. We developed and characterized clinical grade ^{89}Zr-CX-072, which is currently studied in patients as part of a phase I/II clinical trial (NCT03013491) to support CX-072 drug development.

Abstract

Purpose: Probody™ therapeutic CX-072 is a protease-activatable antibody that is cross-reactive with murine and human programmed death-ligand 1 (PD-L1). CX-072 can be activated *in vivo* by proteases present in the tumor microenvironment, thereby potentially reducing peripheral, anti-PD-L1-mediated toxicities. To study its targeting of PD-L1-expressing tissues, we radiolabeled CX-072 with the positron emission tomography (PET) isotope zirconium-89 (^{89}Zr). **Experimental design:** ^{89}Zr-labeled CX-

072, non-specific Probody control molecule (PbCtrl) and CX-072 parental antibody (CX-075) were injected in BALB/c nude mice bearing human MDA-MB-231 tumors or C57BL/6J mice bearing syngeneic MC38 tumors. Mice underwent serial PET imaging 1, 3 and 6 days post intravenous injection (pi), followed by *ex vivo* biodistribution. Intratumoral ^{89}Zr-CX-072 distribution was studied by autoradiography on tumor tissue sections, which were subsequently stained for PD-L1 by immunohistochemistry. Activated CX-072 species in tissue lysates were detected by Western capillary electrophoresis. **Results:** PET imaging revealed ^{89}Zr-CX-072 accumulation in MDA-MB-231 tumors with 2.1-fold higher tumor-to-blood ratios at 6 days pi compared to ^{89}Zr-PbCtrl. Tumor tissue autoradiography showed high ^{89}Zr-CX-072 uptake in high PD-L1-expressing regions. Activated CX-072 species were detected in these tumors, with 5.3-fold lower levels found in the spleen. Furthermore, ^{89}Zr-CX-072 uptake by lymphoid tissues of immune-competent mice bearing MC38 tumors was low compared to ^{89}Zr-CX-075, which lacks the Probody design. **Conclusions:** ^{89}Zr-CX-072 accumulates specifically in PD-L1-expressing tumors with limited uptake in murine peripheral lymphoid tissues. Our data may enable clinical evaluation of ^{89}Zr-CX-072 whole-body distribution as a tool to support CX-072 drug development (NCT03013491).

Introduction

Immunotherapies targeting immune-regulatory checkpoints have acquired a clear role in clinical cancer care. These therapies improve survival of patients with advanced stages of several tumor types, although not all patients respond (1). Immune checkpoint inhibition can elicit a unique spectrum of immune-related adverse events (irAEs) due to

the role of these immune checkpoints in maintaining immunologic homeostasis, including toxicities of endocrine, hepatologic, dermatologic, cardiac and gastro-enteric origin, that can be life-threatening (2). Combining immune checkpoint inhibitors improves response rates and overall survival for specific cancers (3–7), but these combinations often show increases in rate and severity of side-effects (8–10). Immune checkpoint inhibitors with reduced peripheral, immune-related toxicities are therefore of interest.

CX-072 is a Probody™ therapeutic that targets the programmed death-ligand 1 (PD-L1) immune checkpoint. It is currently studied in a phase 1/2 clinical trial (ClinicalTrials.gov identifier NCT03013491). CX-072 potentially limits irAEs, as it is activated preferentially in the tumor microenvironment (11–13). Tumor-associated proteases can remove the masking peptide that blocks the PD-L1-binding region, yielding activated antibody with ~100-fold increased target affinity compared to its intact, inactivated form (Fig. 1).

Due to its design, the CX-072 tissue distribution profile is expected to diverge from other PD-L1-targeting antibodies. Positron-emission tomography (PET) imaging is a powerful, non-invasive technique to determine *in vivo* antibody distribution when used with radiolabeling. It provides quantitative spatial and temporal information on tissue-targeting and target-expression. The PET isotope zirconium-89 (^{89}Zr; $t_{1/2}$ = 78.4 hours) is favorable for radiolabeling antibodies, as its physical half-life matches the time antibodies require for tumor accumulation, resulting in an optimal tumor-to-background signal (14).

Several preclinical imaging studies have reported high uptake of radiolabeled PD-L1-targeting antibodies in murine lymphoid tissues, including spleen, lymph nodes and thymus, but also in brown adipose tissue (BAT) (15,16). PET imaging with radiolabeled anti-PD-L1 antibody ^{89}Zr-atezolizumab in patients measured high, heterogeneous uptake in tumor lesions as well as in spleen, non-malignant lymph nodes and Waldeyer's ring (17).

We performed a PET imaging study in murine models with ^{89}Zr-labeled CX-072 to reveal its whole-body distribution. Also, we compared ^{89}Zr-CX-072-targeting of tumor and lymphoid tissues in both an immune-compromised and an immune-competent setting. To enable clinical PET imaging of ^{89}Zr-CX-072 distribution to tumor and lymphoid tissues in patients, we characterized and developed a good manufacturing practice (GMP) compliant tracer.

Materials and methods

Radiolabeling of CX-072, PbCtrl and CX-075. CX-072, non-specific Probody control molecule (PbCtrl) and parental antibody CX-075 (CytomX Therapeutics) were allowed to react with an 1:2 molar excess of tetrafluorphenol-N-succinyldesferal (TFP-N-sucDf) (ABX GmbH) as described previously (18), with the following modification: pH was set to 4.0-4.5 using 1.0 M ammonium acetate instead of 0.025 M sulfuric acid to prevent aggregate formation. CX-072-N-sucDf, PbCtrl-N-sucDf and CX-075-N-sucDf were purified using a Vivaspin-2 concentrator, aliquoted and stored at -80 °C. Concentration and purity were determined by a Waters size exclusion high-performance liquid chromatography (SE-HPLC) system equipped with a dual-wavelength absorbance

detector (280 nm versus 430 nm), in-line radioactivity detector and TSK-Gel SW column G3000SWXL 5 µm, 7.8 mm (Joint Analytical Systems; mobile phase: phosphate buffered saline (PBS; 9.0 mM sodium phosphate, 1.3 mM potassium phosphate, 140 mM sodium chloride, pH 7.2) (Hospital Pharmacy UMCG); flow: 0.7 mL/min).

CX-072-N-sucDf, PbCtrl-N-sucDf and CX-075-N-sucDf were radiolabeled with clinical grade ^{89}Zr (Perkin Elmer) as described previously (18). Radiochemical purity was assessed by a trichloroacetic acid precipitation assay (19). For all experiments, radiochemical purity of ≥95% was required.

Immunoreactivity. Immunoreactivity after conjugation to TFP-N-SucDf was assessed by indirect enzyme-linked immunosorbent assay (ELISA). 96-well plates (Nunc Maxisorp) were coated with 1 µg/mL human extracellular PD-L1 domain (R&D Systems; 156-B7-100) diluted in PBS (Gibco; 0.7 mM sodium phosphate, 1.5 mM potassium phosphate, 154 mM sodium chloride, pH 7.2) and incubated overnight at 4 °C. Wells were blocked for 2 hours at room temperature (RT) with 1% bovine serum albumin (Sigma-Aldrich), 0.05% Tween 20 in PBS. After blocking, plates were incubated with either unconjugated CX-072, PbCtrl or CX-075 or their respective N-sucDf-conjugates in a concentration ranging from 0.0914 to 600 nM for 60 minutes at RT. Plates were subsequently washed with 0.05% Tween 20 in PBS and incubated with horseradish peroxidase-labeled anti-human IgG antibody (Sigma-Aldrich; A0293) for 60 minutes at RT. Detection was performed with single-component TMB peroxidase substrate (BioRad) and optical density read-out was performed at 450 nm using a micro plate-reader. Immunoreactivity was analyzed by nonlinear regression Log(agonist) vs.

response in Graphpad Prism v7.0. and was expressed as the effective concentration needed for 50% of receptor occupation (EC50).

Cell lines. PD-L1-expressing human triple negative breast cancer cell line MDA-MB-231 was a kind gift from Dr. Janet Price, MD Anderson Cancer Center (Houston, TX). Cell lines were confirmed to be negative for microbial contamination and were authenticated in January 2018 by BaseClear using short tandem repeat profiling. The murine PD-L1 positive colon cancer cell line MC38 was obtained from Dr. Walter Storkus, University of Pittsburgh (Pittsburgh, PA). MDA-MB-231 and MC38 cells were cultured in Dulbecco's modified Eagle medium (Gibco) containing 1.0 g/L glucose and 4.5 g/L glucose respectively, supplemented with 10% fetal calf serum (FCS). Cells were incubated at 37 °C in a humidified atmosphere with 5% CO_2 and were passaged no longer than 6 months. For all experiments, cells were collected in the exponential growth phase.

Flow cytometry. Flow cytometry experiments in MDA-MB-231 and MC38 cells were performed using CX-075 parental antibody, which is cross-reactive to human and murine PD-L1. Cells were trypsinized and harvested in PBS with 2% FCS and kept on ice prior to use. IgG_4 isotype control antibody and CX-075 were diluted in PBS with 2% FCS to 20 µg/mL and incubated with $2*10^5$ cells in 1 mL for 1 hour at 4 °C. Bound primary antibody was detected using a phycoerythrin-conjugated goat anti-human IgG secondary antibody (Southern Biotech; 2040-09) diluted 1:50 in 2% FCS in PBS and analyzed on a BD Accuri C6 flow cytometer (BD Biosciences). Data analysis was performed with FlowJo v10 (Tree Star) and surface receptor expression was expressed as mean fluorescent intensity (MFI).

For flow cytometry experiments in lymphoid tissues, spleen, lymph nodes, bone marrow, BAT and thymus were collected from BALB/c nude and C57BL/6J mice. Single cell suspensions were prepared using a cell strainer (Fisher Scientific). Red blood cell lysis buffer (BioLegend) was used for spleen and bone marrow samples. Single cells were analyzed for PD-L1 expression by flow cytometry, using Brilliant Violet 421™ anti-mouse PD-L1 (CD274) antibody (BioLegend; 124315) and Brilliant Violet 421™ Rat IgG_{2b} isotype control antibody (BioLegend; 400639). Zombie aqua (BioLegend; 423101) was used for detection of viable cells. In splenocytes, PD-L1 expression on specific immune cell types was measured using fluorescein isothiocyanate-conjugated rat anti-mouse CD3 antibody (Thermo Scientific; 11-0032-82) diluted 1:200 in PBS with 2% FCS, allophycocyanin-eFluor780-conjugated rat anti-mouse CD335 antibody (Thermo Scientific; 47-3351-80) diluted 1:20, peridinin chlorophyll protein complex-cyanine5.5-conjugated rat anti-mouse CD11b antibody (Thermo Scientific; 45-0112-80) diluted 1:80, and allophycocyanin-conjugated rat anti-mouse CD19 antibody (Thermo Scientific; 17-0193-80) diluted 1:160. Samples were analyzed on a BD FACS Verse (BD Biosciences). BAT was excluded from measurements, as insufficient amounts of immune cells were present in these samples.

^{89}Zr-CX-075 internalization in MDA-MB-231 and MC38 cell lines. ^{89}Zr-CX-075 was used for internalization experiments since it acts as a surrogate for potential internalization of ^{89}Zr-CX-072 after removal of its masking peptide by tumor-associated proteases. Internalization in MDA-MB-231 and MC38 cells was assessed by adding 50 ng ^{89}Zr-CX-075 (200 MBq/mg) to $1*10^6$ cells. For control of binding without internalization, cells were incubated for 1 hour on ice. Cells were subsequently washed

with ice cold 1% human serum albumin (Sanquin) in PBS. Total PD-L1 bound ^{89}Zr-CX-075 was determined by measuring cell-associated activity in a calibrated well-type gamma counter followed by incubation for 1 and 2 hours at 37 °C, while controls were kept on ice. Cells were stripped of cell-surface bound antibody using 0.05 M glycine and 0.1 M sodium chloride (pH 2.8) and subsequently counted for remaining cell-associated activity, i.e. internalized PD-L1-bound ^{89}Zr-CX-075, in a calibrated well-type gamma counter. Internalization was expressed as percentage of total PD-L1-bound ^{89}Zr-CX-075, corrected for internalization in 4 °C controls.

Animal studies. All animal experiments were performed in accordance with the Dutch code of practice: “Animal experiments in cancer research” and were approved by the institutional animal care and use committee of the University of Groningen, the Netherlands.

PD-L1-expressing MDA-MB-231 human triple negative breast cancer cells were subcutaneously (sc) engrafted in male BALB/cOlaHsd-*Foxn1*^{nu} mice (Envigo). Tumors were allowed to grow 4 weeks, yielding tumor volumes of ±200 mm^3. To study ^{89}Zr-CX-072 target-specific tumor uptake and the potential for antigen saturation, mice received 10 µg ^{89}Zr-CX-072, ^{89}Zr-PbCtrl or ^{89}Zr-CX-075 (~5 MBq) supplemented with 0, 40 or 240 µg of unlabeled CX-072, PbCtrl or CX-075, respectively, via penile vein injection (n = 5-6 per group). To evaluate biodistribution in a fully immune-competent, syngeneic model, male C57BL/6JOlaHsd mice (Envigo) were implanted sc with MC38 murine colon adenocarcinoma cells. After 16 days of tumor growth to reach a volume of ±200 mm^3, mice received 10 µg of ^{89}Zr-CX-072, ^{89}Zr-PbCtrl or ^{89}Zr-CX-075 via penile vein injection (n = 5-6 per group).

Mice underwent serial *in vivo* PET scans 1, 3 and 6 days post intravenous injection (pi) in a Focus 200 microPET scanner (CTI Siemens), followed by tissue collection for *ex vivo* biodistribution analysis. Tissues were weighed and counted in a calibrated well-type gamma counter (LKB instruments). Tracer uptake per organ was quantified by percentage injected dose per gram tissue (%ID/g).

PET data were reconstructed using a 2-dimensional ordered-subset expectation maximization reconstruction algorithm with Fourier rebinning, 4 iterations, and 16 subsets. Data sets were corrected for decay, random coincidences, scatter, and attenuation. PET images were analyzed using AMIDE medical image data examiner software 1.0.5 and regions of interest were drawn for tumor, spleen and blood pool (i.e. heart). Tracer uptake was quantified as mean standardized uptake value (SUV_{mean}).

Tracer integrity. Tracer integrity was studied *ex vivo* by sodium dodecylsulphate polyacrylamide gel electrophoresis (SDS PAGE) in plasma obtained after sacrifice on 6 days pi. Total protein concentration was determined by the Bradford assay (20). Mini-Protean® TGX™ precast protein gels 4-15% (BioRad) were loaded with 40 µg of total plasma protein. As a positive control, freshly radiolabeled (intact) ^{89}Zr-CX-072 was diluted to match activity levels of plasma samples. Gels were allowed to run for 30-45 min at 100 V. Detection was performed by exposing gels to a multipurpose phosphor plate (Perkin Elmer) overnight at -20 °C; exposures were captured using a Cyclone® phosphor imager.

Assessment of activated and intact CX-072 in tumor lysates. Tumor homogenates were prepared in Pierce™ IP lysis buffer (Thermo Scientific) with added Halt™ protease inhibitor cocktail kit (Thermo Scientific) using a Barocycler (Pressure Biosciences).

Protein lysates in IP lysis buffer with protease inhibitor/EDTA were analyzed by the Wes™ system (ProteinSimple). Activated, intact CX-072 was detected using mouse anti-CX-075 primary antibody (CytomX Therapeutics) and anti-mouse secondary antibody (ProteinSimple; 042-205). Concentrations of activated CX-072 were analyzed using Compass software (ProteinSimple).

***Ex vivo* tissue preparation, autoradiography and PD-L1 immunohistochemistry.** For *ex vivo* tissue analysis, paraffin-embedded formalin-fixed (FFPE) tumor tissue blocks were prepared. For autoradiography, FFPE blocks were sliced into 4 µm tumor tissue sections and exposed to a phosphor plate overnight at -20 °C. Exposures were captured using a phosphor imager (Cyclone).

For PD-L1 immunohistochemistry, previously autoradiographed FFPE tumor tissue sections were deparaffinized in xylene and rehydrated. Heat-induced antigen retrieval was performed in 10 mM citrate buffer (pH 6.0) for 15 minutes at 95-100 °C. Endogenous peroxidase was blocked by 10-minute incubation with dual endogenous enzyme-blocking reagent (Agilent Technologies). Slides were rinsed in 137 mM sodium chloride, 20 mM tris(2,3-dibromopropyl) phosphate, 0.1% Tween-20 (pH 7.6) and subsequently incubated with Dako serum free protein block (Agilent Technologies) for 30 minutes at RT. For human PD-L1 staining, slides were incubated with rabbit anti-human PD-L1 antibody (Abcam; ab205921) or rabbit IgG antibody control (Abcam; ab172730) diluted to 5 µg/mL in Dako serum free protein block for 1 hour at RT. Thereafter, slides were incubated with Dako EnVision HRP system (Agilent Technologies) for 30 minutes at RT, followed by 10-minute incubation with diaminobenzidine chromogen. Hematoxylin counterstaining was applied routinely. For

histological analysis of tumors, hematoxylin/eosin staining was performed on tissue sections that were sliced subsequent to the sections used for autoradiography. Digital scans of slides were acquired by a Hamamatsu NanoZoomer 2.0-HT multi slide scanner and analyzed with NanoZoomer Digital Pathology viewer software.

Murine PD-L1 staining was performed as described previously (21). Heat-induced antigen retrieval was performed in 10 mM citrate (pH 6.0) in a Lab Vision™ PT module (Thermo Scientific) at 95 °C. Endogenous peroxidase was blocked by 10-minute incubation at RT with 3% hydrogen peroxide in PBS, followed by 15-minute avidin/biotin-blocking (Vector Labs). Slides were preincubated with 10% Dako normal rabbit serum (Agilent Technologies) for 30 minutes at RT. Goat anti-mouse PD-L1 antibody (R&D systems; AF1019) or normal goat IgG control antibody (R&D systems; AB-108-C) diluted to 0.4 µg/mL in PBS with 1% bovine serum albumin (BSA) was incubated overnight at 4 °C, followed by 30-minute incubation at RT with rabbit anti-goat biotinylated secondary antibody (Agilent Technologies; E046601-2) diluted 1:400 in PBS with 1% BSA. For detection, slides were incubated with Vectastain Elite ABC HRP-kit (Vector Labs) for 30 minutes at RT.

Production of clinical grade ^{89}Zr-CX-072 and stability testing. Methods for conjugation and radiolabeling were transferred to GMP environment. Analytical procedures were validated to demonstrate suitability for use in quality control testing of CX-072-N-sucDf and ^{89}Zr-CX-072. For validation of the manufacturing process, three batches of GMP compliant CX-072-N-sucDf intermediate product were produced and radiolabeled with ^{89}Zr. For quality control, these batches met specifications on conjugation ratio, activity yield, purity, concentration, pH, radiochemical purity, residual

solvents, sterility and endotoxin content. Preservation of immunoreactivity after conjugation was determined by ELISA as previously described for preclinical conjugated CX-072.

CX-072-N-sucDf intermediate product was stored in sterile vials (Biopure) at -80 °C. Stability of CX-072-N-sucDf batch 1 was analyzed at 0, 1, 3, 6 and 12 months after production. Quality control was performed after radiolabeling with ^{89}Zr according to release specifications.

Statistical analysis. Data were analyzed for statistical significance in GraphPad Prism v7.0 using the Mann-Whitney U test for non-parametric data followed by Bonferroni post-test correction for comparison of more than two groups. Experiments were performed at least three times. *P* values < 0.05 were considered significant.

Results

CX-072 characterization and binding

CX-072, a recombinant, protease-activatable antibody targeting PD-L1, is based on CX-075, a phage-derived, fully human IgG_4 antibody that blocks interactions of PD-L1 with PD-1 and B7-1 molecules. In its intact form, both light chains of CX-072 are modified at their N-terminus by addition of a peptide prodomain, which serves to mask the PD-L1-binding region of the antibody. Proteolytic cleavage of the substrate within the prodomain yields the active, PD-L1-binding form of CX-072.

Binding of CX-075 parental antibody, which lacks a masking peptide, was comparable for both human (K_{app} = 0.25 nM) and murine (K_{app} = 0.30 nM) PD-L1 (Supplementary Fig. S1A), whereas CX-072 binding to murine PD-L1 was ~15-fold

weaker than for human PD-L1. CX-072 bound to murine PD-L1 at K_{app} of 152 nM and bound to human PD-L1 at K_{app} of 9.9 nM, as determined by ELISA (Supplementary Fig. S1B).

In vivo ^{89}Zr-CX-072 tumor and spleen uptake over time

For *in vivo* PET imaging studies, CX-072, PbCtrl and CX-075 were conjugated to an average of ~1.2 TFP-N-sucDf chelators per antibody and thereafter radiolabeled with 500 MBq/mg ^{89}Zr at ≥95% radiochemical purity. Immunoreactivity to PD-L1 was preserved for CX-072-N-sucDf and CX-075-N-sucDf, while PbCtrl-N-sucDf remained non-avid (Supplementary Fig. S1C, D).

To study human tumor-targeting, we performed *in vivo* studies in human PD-L1-expressing MDA-MB-231 xenograft tumor-bearing BALB/c nude mice. In this model, we compared tumor-targeting with targeting of the spleen, since this lymphoid organ is well-developed in immune-compromised mice and can be quantified with imaging. Serial PET scans on days 1, 3 and 6 pi showed tumor accumulation over time for ^{89}Zr-CX-072 and ^{89}Zr-CX-075, but not for ^{89}Zr-PbCtrl (Fig. 2A). PET quantification revealed a 1.5-fold higher spleen uptake for ^{89}Zr-CX-075 than for ^{89}Zr-CX-072 at day 6 pi ($p < 0.01$). ^{89}Zr-CX-075 spleen uptake was already higher than blood pool levels at day 1 pi and increased to a spleen-to-blood ratio of 2.6 ± 0.5 at day 6 pi (Fig. 2B), suggesting this uptake is PD-L1-mediated. Tracer activity in the blood pool decreased over time, resulting in increasing tumor-to-blood ratios for ^{89}Zr-CX-072 and ^{89}Zr-CX-075 from day 1 to 6 pi with highest tumor uptake observed at day 6 pi. Day 6 was selected for *ex vivo* biodistribution studies of subsequent mouse cohorts based on highest ^{89}Zr-CX-072 tumor-to-blood ratio of 0.9 ± 0.2, compared to 0.4 ± 0.0 found for ^{89}Zr-PbCtrl ($p < 0.01$).

Ex vivo ^{89}Zr-CX-072 biodistribution in tumor-bearing mice

Ex vivo tracer uptake quantitation per organ revealed similar biodistribution of ^{89}Zr-CX-072 and ^{89}Zr-PbCtrl in healthy, non-tumor tissues (Fig. 3A). Compared to ^{89}Zr-CX-072, blood pool levels and uptake in the heart were lower for ^{89}Zr-CX-075, whereas its uptake in liver, pancreas, stomach, ilium, bone, skin and spleen was higher.

Next, we assessed whether tracer uptake in tumor and spleen is PD-L1-mediated through a protein dose-escalation study. A radiolabeled antibody dose of 10 µg ^{89}Zr-CX-072, ^{89}Zr-PbCtrl or ^{89}Zr-CX-075 was supplemented with 0, 40 or 240 µg of unlabeled CX-072, PbCtrl or CX-075 to obtain total protein doses of 10 µg, 50 µg and 250 µg for each tracer. We found that ^{89}Zr-CX-072 and ^{89}Zr-PbCtrl biodistribution in healthy tissues was not affected by increased protein dose, but ^{89}Zr-CX-075 uptake in these healthy organs decreased with increasing total protein dose (Supplementary Fig. S2). PET quantification showed blood pool levels of all three radiolabeled molecules were unaffected by increased protein dose (Supplementary Fig. S3).

Ex vivo tracer uptake quantitation showed a protein dose-dependent tumor uptake for ^{89}Zr-CX-072 and ^{89}Zr-CX-075, which was not observed for ^{89}Zr-PbCtrl (Fig. 3B). ^{89}Zr-CX-072 tumor uptake decreased from 8.7 ± 1.0 %ID/g for the 10 µg total protein dose to 6.0 ± 1.3 %ID/g and 4.3 ± 0.7 %ID/g for the 50 µg and 250 µg dose groups, respectively, indicating competition of tracer with unlabeled CX-072 for PD-L1 receptor-binding. This shows ^{89}Zr-CX-072 tumor uptake is PD-L1-driven. Similarly, ^{89}Zr-CX-075 tumor uptake was reduced by unlabeled antibody. ^{89}Zr-PbCtrl tumor uptake was independent of total protein dose, confirming its non-specificity for PD-L1.

Although immune-compromised mice were used for this model, PD-L1-mediated spleen uptake was observed for ^{89}Zr-CX-075. Spleen uptake of ^{89}Zr-CX-075 decreased from 25.8 ± 4.1 %ID/g at the 10 µg total protein dose to 10.8 ± 2.8 %ID/g for the 50 µg dose group and 5.3 ± 2.6 %ID/g for the 250 µg dose group. ^{89}Zr-CX-072 did not show protein dose-dependent spleen uptake, similar to ^{89}Zr-PbCtrl, indicating this spleen uptake is not PD-L1-driven, but part of normal, non-specific antibody distribution.

^{89}Zr-CX-072 and ^{89}Zr-CX-075 showed a comparable tumor uptake of 8.7 ± 1.0 %ID/g and 8.8 ± 2.9 %ID/g, respectively, for the 10 µg total protein dose, whereas only 3.8 ± 0.2 %ID/g was observed for 10 µg ^{89}Zr-PbCtrl. This demonstrates that CX-072's design affects biodistribution to healthy organs, but not its tumor-targeting properties.

Tumor-specific activation of CX-072 species

MDA-MB-231 tumor and spleen lysates were analyzed for presence of activated CX-072 to confirm whether CX-072 is specifically activated by proteases in the tumor microenvironment. Flow cytometry revealed PD-L1 expression by MDA-MB-231 tumor cells and splenocytes of BALB/c nude mice (Fig. 3C). Immunohistochemistry on *ex vivo* tumor and spleen tissues also confirmed presence of PD-L1. MDA-MB-231 tumor lysates had 6.9 ng/mL activated CX-072 species at the 10 µg total protein dose, 21.2 ng/mL at the 50 µg total protein dose, and highest concentration of 81.7 ng/mL was found for the 250 µg dose group (Fig. 3D). Activated CX-072 levels detected in spleen lysates at the 250 µg total protein dose was 5.3-fold lower compared to tumor lysates ($p < 0.05$). This demonstrates that CX-072 is preferentially activated in tumor tissue and thereafter remains predominantly within the tumor microenvironment. Furthermore,

circulating ^{89}Zr-CX-072 tracer remained intact in the blood pool at 6 days pi, as confirmed by SDS-PAGE (Fig. 3E).

^{89}Zr-CX-072 targeting of tumor and lymphoid tissues in a syngeneic mouse model

To assess ^{89}Zr-CX-072-targeting of relevant PD-L1-expressing tissues besides tumor, tracer distribution in BALB/c nude mice was compared with fully immune-competent C57BL/6J mice bearing murine PD-L1-expressing MC38 tumors. PET imaging at 6 days pi revealed high spleen uptake for ^{89}Zr-CX-075 in both mouse models, which was not visible for ^{89}Zr-CX-072 and ^{89}Zr-PbCtrl (Fig. 4A). Importantly, ^{89}Zr-CX-072 and ^{89}Zr-CX-075 showed comparable uptake in syngeneic MC38 tumors at 6 days pi (Supplementary Fig. S4A), while 3.1-fold higher spleen uptake was observed for ^{89}Zr-CX-075 compared to ^{89}Zr-CX-072 in C57BL/6J mice ($p < 0.01$).

PD-L1-expression in spleen, mesenteric lymph nodes, axillary lymph nodes, BAT and thymus was confirmed by immunohistochemistry and flow cytometry (Fig. 4B, Fig. 5A). Although limited immune cells were found in BAT, immunohistochemistry revealed PD-L1 expression by adipocytes. High ^{89}Zr-CX-075 uptake was found in these peripheral PD-L1-expressing tissues *ex vivo* (Fig 4C). In contrast, ^{89}Zr-CX-072 uptake was low in these tissues and comparable to ^{89}Zr-PbCtrl, indicating that CX-072's design limits uptake in lymphoid tissues and BAT. Notably, ^{89}Zr-CX-075 spleen uptake was comparable in both tumor-bearing BALB/c nude and C57BL/6J mice. We found few T cells among BALB/c nude mouse splenocytes, while monocytes, NK cells and B cells were abundant and showed high levels of PD-L1 expression (Fig. 5B).

Ex vivo ^{89}Zr-CX-072 uptake was higher in MDA-MB-231 tumors compared to MC38 tumors (Supplementary Fig. S5). Flow cytometry confirmed MDA-MB-231 and

MC38 cell lines both express PD-L1 *in vitro*, albeit at a higher level in MDA-MB-231 cells (Supplementary Fig. S5A, B). After 2 hours of incubation, 31.7 ±1.2% of PD-L1-bound ^{89}Zr-CX-075 was internalized in MDA-MB-231 cells (Supplementary Fig. S5C). This finding supports the idea that ^{89}Zr-CX-072 tracer activity can residualize in the tumor after removal of its masking peptide. Tracer internalization and ^{89}Zr residualization may augment the PET signal, resulting in better tumor visualization. Negligible internalization was found for PD-L1-bound ^{89}Zr-CX-075 in MC38 cells: 2.5 ±0.5% after 2 hours of incubation. Low levels of PD-L1 expression combined with limited internalization in MC38 tumors may explain why the observed ^{89}Zr-CX-072 tumor uptake was not significantly different from ^{89}Zr-PbCtrl (Supplementary Fig. S5D).

Similar to our observations in BALB/c nude tumor-bearing mice, *ex vivo* tracer uptake quantitation in C57BL/6J tumor-bearing mice revealed comparable biodistribution in healthy organs for ^{89}Zr-CX-072 and ^{89}Zr-PbCtrl (Supplementary Fig. S4B). ^{89}Zr-CX-075 uptake was higher in liver, ilium and brain, while blood pool levels were lower compared to ^{89}Zr-CX-072. ^{89}Zr-CX-075 is potentially affected by target-mediated drug disposition, while ^{89}Zr-CX-072 is not, presumably due to protection by its masking peptide. Additionally, residual activity measured in tumor-bearing mice at 1, 3 and 6 days pi suggests a slightly faster metabolism for ^{89}Zr-CX-075 compared to ^{89}Zr-CX-072 (Supplementary Fig. S6).

^{89}Zr-CX-072 tumor uptake on autoradiography correlates to PD-L1-expressing tissue

Finally, we studied *ex vivo* macroscopic tracer distribution in FFPE tumor tissue slices using autoradiography to further confirm PD-L1-specific tumor-targeting.

Autoradiography revealed a heterogeneous distribution pattern for ^{89}Zr-CX-072 and ^{89}Zr-CX-075, but not for ^{89}Zr-PbCtrl (Fig. 6). PD-L1 staining was observed in both viable and necrotic tumor tissue and correlated to regions showing high uptake of ^{89}Zr-CX-072 on autoradiography. Tumor tissue regions showing low ^{89}Zr-CX-072 uptake on autoradiography had corresponding low levels of PD-L1 expression. In contrast, ^{89}Zr-PbCtrl distributed to non-tumor areas while PD-L1 expression was present in viable tumor tissue, indicating that the observed uptake is not PD-L1-specific. ^{89}Zr-CX-075 also distributed to tumor tissue regions expressing high levels of PD-L1.

Clinical grade ^{89}Zr-CX-072 for patient studies

To enable PET imaging in patients, we optimized and validated a robust, GMP compliant manufacturing process for clinical grade ^{89}Zr-CX-072. Three validation batches of clinical grade CX-072-N-sucDf intermediate product were produced and subsequently radiolabeled with ^{89}Zr, which met prior set quality specifications. CX-072-N-sucDf intermediate product demonstrated stability up to 12 months. Therefore, CX-072-N-sucDf shelf-life is currently set at 12 months and may be extended if the product remains within specifications at future time points. An investigational medicinal product dossier (IMPD) for ^{89}Zr-CX-072 was compiled, submitted and approved by the competent authority as part of clinical trial application. A clinical study evaluating ^{89}Zr-CX-072 biodistribution in patients is currently ongoing at our center as part of the CX-072 phase 1/2 study.

Discussion

This study demonstrates that ^{89}Zr-CX-072 is activated in tumor tissue, followed by PD-L1-mediated tumor uptake, whereas PD-L1-mediated accumulation in healthy, peripheral PD-L1-expressing tissues is limited. Importantly, we found comparable tumor uptake for ^{89}Zr-CX-072 and its parental antibody ^{89}Zr-CX-075 in both human xenograft and syngeneic tumor-bearing mice, indicating that CX-072's required activation by proteases does not hamper tumor uptake.

Low uptake of ^{89}Zr-CX-072 was found in PD-L1-expressing lymphoid tissues and BAT, similar to ^{89}Zr-labeled non-specific Probody control molecule, which shows this uptake is not mediated by PD-L1. This finding is remarkably different from lymphoid tissue-targeting properties of other antibodies whose PD-L1-binding regions are not masked. PD-L1 is abundantly expressed by subsets of immune cells present in healthy lymphoid tissues of mice and humans (15,22). As a consequence, PD-L1-targeting antibodies generally show high uptake in the spleen, which potentially affects their biodistribution and pharmacokinetic profile. Several preclinical imaging studies using radiolabeled, PD-L1-targeting antibodies in tumor-bearing mice have reported high tracer uptake in the spleen (15,16,21,23–29). PET imaging of PD-L1 in cancer patients clearly demonstrated high ^{89}Zr-atezolizumab uptake in the spleen among other lymphoid tissues (17).

Most preclinical PD-L1-imaging studies have used radiolabeled antibodies specific for either murine or human PD-L1 (15,16,21,25,27,28,30). ^{89}Zr-CX-072 human/murine cross-reactivity enabled us not only to evaluate its human tumor-targeting, but also to acquire data on its uptake in murine lymphoid tissues. Peripheral PD-L1 expression in healthy organs, including lymphoid tissues, strongly affected

biodistribution of ^{89}Zr-CX-075 parental antibody, but not biodistribution of ^{89}Zr-CX-072 in tumor-bearing BALB/c nude mice. However, lymphoid tissues in such immune-compromised mice are underdeveloped, leading to absence or anomalous frequencies of specific immune cell types. To overcome this drawback, we used syngeneic MC38 tumor-bearing, immune-competent C57BL/6J mice to study CX-072's biodistribution in greater detail.

Interestingly, PET scans and *ex vivo* biodistribution revealed high uptake of ^{89}Zr-CX-075 parental antibody in spleen and lymph nodes in both BALB/c nude and C57BL/6J mice. Few T cells were present in BALB/c nude mice, but B cells, NK cells and macrophages were abundant and have been shown to be fully functional (31). We found that PD-L1 is highly expressed by monocytes of BALB/c nude mice, in line with previous research (32). B cells and NK cells also demonstrated PD-L1 expression, but only limited amounts of PD-L1 were present on T cells. Nevertheless, BALB/c nude mice demonstrated levels of PD-L1 expression comparable to immune-competent mice. This shows that even though BALB/c nude mice lack a fully functional immune system, they were well-suited for studying ^{89}Zr-CX-072-targeting of lymphoid tissues, and potentially for other PD-L1-targeting antibodies.

^{89}Zr-CX-072 tumor-specific uptake depends on high protease activity within the tumor microenvironment and limited protease levels in healthy organs, including PD-L1-expressing lymphoid tissues (11,12). Proteases that can activate CX-072 are generally up-regulated during tumorigenesis. They include urokinase-type plasminogen activator (uPA), matriptase (MT-SP1) and selected matrix metalloproteinases, which are all associated with many types and stages of cancer (33–37). As an indirect read-out of

protease activity in the tumor microenvironment, we measured high concentrations of activated CX-072 in tumor lysates. This indicates that sufficient levels of proteases were present in tumor tissue to activate CX-072.

Our conclusions are limited by the fact that CX-072, in its intact form, binds with lower affinity to murine PD-L1 compared to human PD-L1. This finding suggests that the masking peptide has greater ability to block CX-072 binding to murine PD-L1. However, once ^{89}Zr-CX-072 is activated, the tracer has similar binding affinity for both murine and human PD-L1. Uptake in PD-L1-expressing lymphoid tissues may be higher in the human setting than we found in mice if large amounts of inactivated ^{89}Zr-CX-072 are taken up by these tissues. Clinical ^{89}Zr-CX-072 PET imaging will reveal whether the tumor-specific activation we observed in mouse models is translatable to patients. To this end, we validated the production process of a GMP compliant ^{89}Zr-CX-072 tracer for clinical PET imaging as a tool to support CX-072 drug development.

In conclusion, we found that ^{89}Zr-CX-072 accumulates specifically in PD-L1-expressing tumor xenografts with limited uptake in murine peripheral lymphoid tissues and BAT, thus supporting the hypothesis that CX-072 may reduce anti-PD-L1-mediated toxicities in these healthy tissues.

Acknowledgments

We thank Linda Pot-de Jong (University Medical Center Groningen) for assistance in the validation and production processes of clinical grade ^{89}Zr-CX-072, Shanti Davur, Eric Ureno and Sridhar Viswanathan (CytomX Therapeutics) for assistance with production and characterization of ^{89}Zr-CX-072 and ^{89}Zr-PbCtrl, and Gerwin Sandker

(Radboud University Medical Center) for helping with immunohistochemistry on murine PD-L1. Research support from CytomX Therapeutics was made available to the institution. The study drug and control molecules were supplied by CytomX Therapeutics.

References

1. Balar A V., Galsky MD, Rosenberg JE, Powles T, Petrylak DP, Bellmunt J, et al. Atezolizumab as first-line treatment in cisplatin-ineligible patients with locally advanced and metastatic urothelial carcinoma: A single-arm, multicentre, phase 2 trial. Lancet. 2017;389:67–76.
2. Postow MA, Sidlow R, Hellmann MD. Immune-related adverse events associated with immune checkpoint blockade. N Engl J Med. 2018;378:158–68.
3. Fucà G, de Braud F, Di Nicola M. Immunotherapy-based combinations. Curr Opin Oncol. 2018;30:345–51.
4. Wolchok JD, Chiarion-Sileni V, Gonzalez R, Rutkowski P, Grob JJ, Cowey CL, et al. Overall survival with combined nivolumab and ipilimumab in advanced melanoma. N Engl J Med. 2017;377:1345–56.
5. Hellmann MD, Ciuleanu T-E, Pluzanski A, Lee JS, Otterson GA, Audigier-Valette C, et al. Nivolumab plus ipilimumab in lung cancer with a high tumor mutational burden. N Engl J Med. 2018;378:2093–104.
6. Overman MJ, Lonardi S, Wong KYM, Lenz H-J, Gelsomino F, Aglietta M, et al. Durable clinical benefit with nivolumab plus ipilimumab in DNA mismatch repair-deficient/microsatellite instability-high metastatic colorectal cancer. J Clin Oncol.

2018;36:773–9.

7. Motzer RJ, Tannir NM, McDermott DF, Arén Frontera O, Melichar B, Choueiri TK, et al. Nivolumab plus ipilimumab versus sunitinib in advanced renal-cell carcinoma. N Engl J Med. 2018;378:1277–90.
8. Larkin J, Chiarion-Sileni V, Gonzalez R, Grob JJ, Cowey CL, Lao CD, et al. Combined nivolumab and ipilimumab or monotherapy in untreated melanoma. N Engl J Med. 2015;373:23–34.
9. Yang H. Safety and efficacy of durvalumab (MEDI4736) in various solid tumors. Drug Des Development Ther. 2018;12:2085–96.
10. Fumet J-D, Isambert N, Hervieu A, Zanetta S, Guion J-F, Hennequin A, et al. Phase Ib/II trial evaluating the safety, tolerability and immunological activity of durvalumab (MEDI4736) (anti-PD-L1) plus tremelimumab (anti-CTLA-4) combined with FOLFOX in patients with metastatic colorectal cancer. ESMO Open. 2018;3:e000375.
11. Desnoyers LR, Vasiljeva O, Richardson JH, Yang A, Menendez EEM, Liang TW, et al. Tumor-specific activation of an EGFR-targeting probody enhances therapeutic index. Sci Transl Med. 2013;5:1–10.
12. Wong KR, Menendez E, Craik CS, Kavanaugh WM, Vasiljeva O. In vivo imaging of protease activity by Probody therapeutic activation. Biochimie. 2016;122:62–7.
13. Wong C, Mei L, Wong KR, Menendez EEM, Vasiljeva O, Richardson JH, et al. A PD-L1-targeted Probody provides antitumor efficacy while minimizing induction of systemic autoimmunity. Cancer Immunology Res. 2016;4(1 suppl): abstract A081.
14. Williams S. Tissue distribution studies of protein therapeutics using molecular

probes: Molecular imaging. Am Assoc Pharm Sci. 2012;14:389–99.

15. Hettich M, Braun F, Bartholomä MD, Schirmbeck R, Niedermann G. High-resolution PET imaging with therapeutic antibody-based PD-1/PD-L1 checkpoint tracers. Theranostics. 2016;6:1629–40.

16. Josefsson A, Nedrow JR, Park S, Banerjee SR, Rittenbach A, Jammes F, et al. Imaging, biodistribution, and dosimetry of radionuclide-labeled PD-L1 antibody in an immunocompetent mouse model of breast cancer. Cancer Res. 2016;76:472–9.

17. Bensch F, van der Veen EL, Lub-de Hooge MN, Jorritsma-Smit A, Boellaard R, Kok IC, et al. ^{89}Zr-atezolizumab imaging as a non-invasive approach to assess clinical response to PD-L1 blockade in cancer. Nat Med. 2018;24:1852–8.

18. Verel I, Visser GWM, Boellaard R, van Walsum-Stigter M, Snow GB, van Dongen GAMS. ^{89}Zr immuno-PET: Comprehensive procedures for the production of ^{89}Zr-labeled monoclonal antibodies. J Nucl Med. 2003;44:1271–81.

19. Nagengast WB, de Vries EGE, Hospers GA, Mulder NH, de Jong JR, Hollema H, et al. In vivo VEGF imaging with radiolabeled bevacizumab in a human ovarian tumor xenograft. J Nucl Med. 2007;48:1313–9.

20. Bradford MM. A rapid and sensitive method for the quantitation of microgram quantities of protein utilizing the principle of protein-dye binding. Anal Biochem. 1976;72:248–54.

21. Heskamp S, Wierstra PJ, Molkenboer-Kuenen JD, Sandker GW, Thordardottir S, Cany J, et al. PD-L1 microSPECT/CT imaging for longitudinal monitoring of PD-L1 expression in syngeneic and humanized mouse models for cancer. Cancer

Immunol Res. 2018;7:150–61.

22. Sun C, Mezzadra R, Schumacher TN. Regulation and function of the PD-L1 checkpoint. Immunity. 2018;48:434–52.

23. Truillet C, Oh HLJ, Yeo SP, Lee CY, Huynh LT, Wei J, et al. Imaging PD-L1 expression with immunoPET. Bioconjug Chem. 2018;29:96–103.

24. Chatterjee S, Lesniak WG, Gabrielson M, Lisok A, Wharram B, Sysa-Shah P, et al. A humanized antibody for imaging immune checkpoint ligand PD-L1 expression in tumors. Oncotarget. 2016;7:10215–27.

25. Li D, Cheng S, Zou S, Zhu D, Zhu T, Wang P, et al. Immuno-PET imaging of ^{89}Zr-labeled anti-PD-L1 domain antibody. Mol Pharm. 2018;15:1674–81.

26. Lesniak WG, Chatterjee S, Gabrielson M, Lisok A, Wharram B, Pomper MG, et al. PD-L1 detection in tumors using ^{64}Cu-atezolizumab with PET. Bioconjug Chem. 2016;27:2103–10.

27. Nedrow JR, Josefsson A, Park S, Ranka S, Roy S, Sgouros G. Imaging of programmed cell death ligand 1: Impact of protein concentration on distribution of anti-PD-L1 SPECT agents in an immunocompetent murine model of melanoma. J Nucl Med. 2017;58:1560–6.

28. Kikuchi M, Clump DA, Srivastava RM, Sun L, Zeng D, Diaz-Perez JA, et al. Preclinical immunoPET/CT imaging using Zr-89-labeled anti-PD-L1 monoclonal antibody for assessing radiation-induced PD-L1 upregulation in head and neck cancer and melanoma. Oncoimmunology. 2017;6:1–13.

29. Jagoda EM, Vasalatiy O, Basuli F, Opina ACL, Williams MR, Wong K, et al. Immuno-PET imaging of the programmed cell death-1 ligand (PD-L1) using a

zirconium-89 labeled therapeutic antibody, avelumab. Mol Imaging. 2019;18:1–14.

30. Heskamp S, Hobo W, Molkenboer-Kuenen JDM, Olive D, Oyen WJG, Dolstra H, et al. Noninvasive imaging of tumor PD-L1 expression using radiolabeled anti-PD-L1 antibodies. Cancer Res. 2015;75:2928–36.
31. Belizário JE. Immunodeficient mouse models: An overview. Open Immunol J. 2009;2:79–85.
32. Hartley G, Regan D, Guth A, Dow S. Regulation of PD-L1 expression on murine tumor-associated monocytes and macrophages by locally produced TNF-α. Cancer Immunol Immunother. 2017;66:523–35.
33. Ulisse S, Baldini E, Sorrenti S, D'Armiento M. The urokinase plasminogen activator system: A target for anti-cancer therapy. Curr Cancer Drug Targets. 2009;9:32–71.
34. Vasiljeva O, Hostetter DR, Moore SJ, Winter MB. The multifaceted roles of tumor-associated proteases and harnessing their activity for prodrug activation. Biol Chem. 2019;400:965–77.
35. Overall CM, Kleifeld O. Validating matrix metalloproteinases as drug targets and anti-targets for cancer therapy. Nat Rev. 2006;6:227–39.
36. Kessenbrock K, Plaks V, Werb Z. Matrix metalloproteinases: Regulators of the tumor microenvironment. Cell. 2010;141:52–67.
37. LeBeau AM, Lee M, Murphy ST, Hann BC, Warren RS, Delos Santos R, et al. Imaging a functional tumorigenic biomarker in the transformed epithelium. Proc Natl Acad Sci. 2013;110:93–8.

Authors' contributions

D. Giesen, L. N. Broer, M. N. Lub-de Hooge, M. Nguyen, O. Vasiljeva, E. G. E. de Vries and M. Pool participated in the design and/or interpretation of the reported experiments or results. D. Giesen, L. N. Broer, M. N. Lub-de Hooge, O. Vasiljeva, E. G. E. de Vries and M. Pool participated in the acquisition and/or analysis of data. I. Popova, B. Howng and O. Vasiljeva analyzed immunoreactivity and presence of activated drug. All authors participated in drafting and/or revising the manuscript. D. Giesen, L. N. Broer, M. N. Lub-de Hooge, O. Vasiljeva, E. G. E. de Vries and M. Pool provided administrative, technical or supervisory support.

Data and materials availability

Data that support the findings of this study are available from E. G. E. de Vries upon request.

Abbreviations

^{89}Zr	zirconium-89
BAT	brown adipose tissue
FFPE	formalin-fixed paraffin-embedded
GMP	good manufacturing practice
ID	injected dose
irAEs	immune-related adverse events

PET	positron emission tomography
PD-L1	programmed death-ligand 1
SUV_{mean}	mean standardized uptake value
TFP-N-sucDf	tetrafluorphenol-N-succinyldesferal

Supplementary materials

Figure S1. CX-072, PbCtrl and CX-075 binding properties.

Figure S2. *Ex vivo* biodistribution with escalating protein dose of ^{89}Zr-CX-072, ^{89}Zr-PbCtrl and ^{89}Zr-CX-075.

Figure S3. *In vivo* quantification of ^{89}Zr-CX-072, ^{89}Zr-PbCtrl and ^{89}Zr-CX-075 PET imaging.

Figure S4. PET imaging and biodistribution in syngeneic MC38 tumor-bearing mice.

Figure S5. *In vitro* PD-L1 expression versus *ex vivo* uptake in MC38 and MDA-MB-231 tumors.

Figure S6. *In vivo* kinetics of ^{89}Zr-CX-072, ^{89}Zr-PbCtrl and ^{89}Zr-CX-072.

Figure legends

Figure 1.

CX-072 mechanism of action. Schematic overview of the CX-072 mechanism of action in healthy and tumor tissues. Both light chains of the anti-PD-L1 parental antibody are

modified at their N-termini by addition of a protease-cleavable linker peptide that tethers a mask to the antibody. In healthy tissue, this mask prevents binding of CX-072 to PD-L1. The masking peptide is removed by proteases commonly up-regulated in the tumor microenvironment, yielding fully activated, PD-L1-targeting antibody.

Figure 2.

***In vivo* tumor and spleen accumulation over time in MDA-MB-231 tumor-bearing mice. (A)** Representative coronal PET images of 10 µg ^{89}Zr-CX-072, ^{89}Zr-PbCtrl and ^{89}Zr-CX-075 in MDA-MB-231 tumor-bearing mice at 1, 3 and 6 days pi. Tracer uptake is presented as standardized uptake value (SUV). H: heart, T: tumor, S: spleen. **(B)** PET imaging quantification of ^{89}Zr-CX-072, ^{89}Zr-PbCtrl and ^{89}Zr-CX-075 uptake in MDA-MB-231 tumor, blood pool (surrogated by heart) and spleen at 1, 3 and 6 days pi. Tracer uptake is presented as mean standardized uptake value (SUV_{mean}). Data is shown as mean ± standard deviation (SD).

Figure 3.

***Ex vivo* biodistribution in MDA-MB-231 tumor-bearing mice. (A)** *Ex vivo* biodistribution of 10 µg ^{89}Zr-CX-072, ^{89}Zr-PbCtrl and ^{89}Zr-CX-075 in MDA-MB-231 tumor-bearing mice at 6 days pi. Tracer uptake per organ is presented as %ID/g. Data is shown as mean ± SD. **(B)** *Ex vivo* tumor and spleen uptake of ^{89}Zr-CX-072, ^{89}Zr-PbCtrl and ^{89}Zr-CX-075 at increasing total protein dose. Tracer uptake is presented as %ID/g. Data is shown as mean ± SD. **(C)** PD-L1 expression in MDA-MB-231 cells and

splenocytes detected with flow cytometry and in FFPE tumor and spleen tissue sections detected with immunohistochemistry. IgG_4 antibody was used as isotype control. **(D)** Activated CX-072 species detected *ex vivo* in MDA-MB-231 tumor tissue and spleen by Western capillary electrophoresis. Data is shown as mean ± SD. **(E)** *Ex vivo* tracer integrity of ^{89}Zr-CX-072 in plasma samples 6 days pi, as determined by SDS PAGE. Detection of signal was performed by autoradiography. Data from a representative experiment is shown. **: $p < 0.01$, *: $p < 0.05$, ns: not significant.

Figure 4.

Biodistribution in tumor-bearing BALB/c nude and C57BL/6J mice. (A) Representative maximum intensity projections of ^{89}Zr-CX-072, ^{89}Zr-PbCtrl and ^{89}Zr-CX-075 in MC38 tumor-bearing C57BL/6J mice and MDA-MB-231 tumor-bearing BALB/c nude mice imaged at 6 days pi. H: heart, T: tumor, S: spleen. **(B)** PD-L1 immunohistochemistry in lymphoid tissues of tumor-bearing BALB/c nude and C57BL/6J mice. MLN: mesenteric lymph nodes, ALN: axillary lymph nodes, BAT: brown adipose tissue. **(C)** *Ex vivo* uptake of ^{89}Zr-CX-072, ^{89}Zr-PbCtrl and ^{89}Zr-CX-075 in lymphoid tissues of BALB/c nude and C57BL/6J mice at 6 days pi. Tracer uptake per organ is presented as %ID/g. Data is shown as mean ± SD. *: $p < 0.05$; **: $p < 0.01$; ns: not significant.

Figure 5.

PD-L1 expression by specific immune cells types in BALB/c nude and C57BL/6J mice. (A) PD-L1 expression detected with flow cytometry in single-cell suspensions of BALB/c nude and C57BL/6J lymphoid tissues. LN: lymph nodes, BM: bone marrow. **(B)** Within splenocytes, PD-L1 expression was measured on specific immune cells types using flow cytometry.

Figure 6.

***Ex vivo* macroscopic tumor tissue distribution.** Autoradiography images of ^{89}Zr-CX-072, ^{89}Zr-PbCtrl and ^{89}Zr-CX-075 in FFPE MDA-MB-231 tumor tissue sections, followed by PD-L1 immunohistochemistry. Hematoxylin/eosin (H&E) staining was performed on an adjacent tissue section to demonstrate viability of tumor tissue. Representative data is shown.

Figure 1

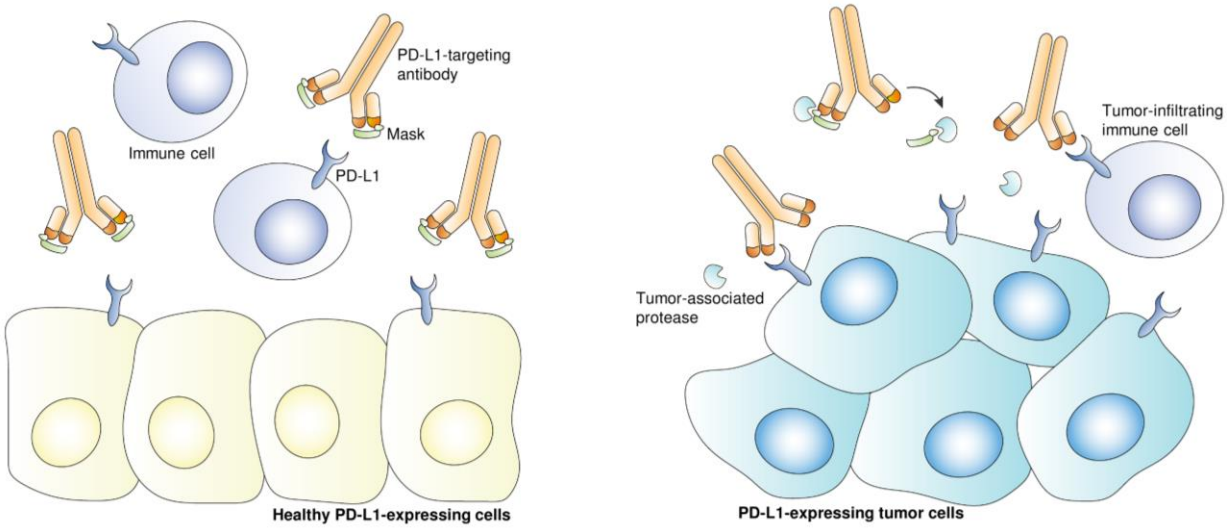

Author Manuscript Published OnlineFirst on January 17, 2020; DOI: 10.1158/1078-0432.CCR-19-3137
Author manuscripts have been peer reviewed and accepted for publication but have not yet been edited.

Figure 2

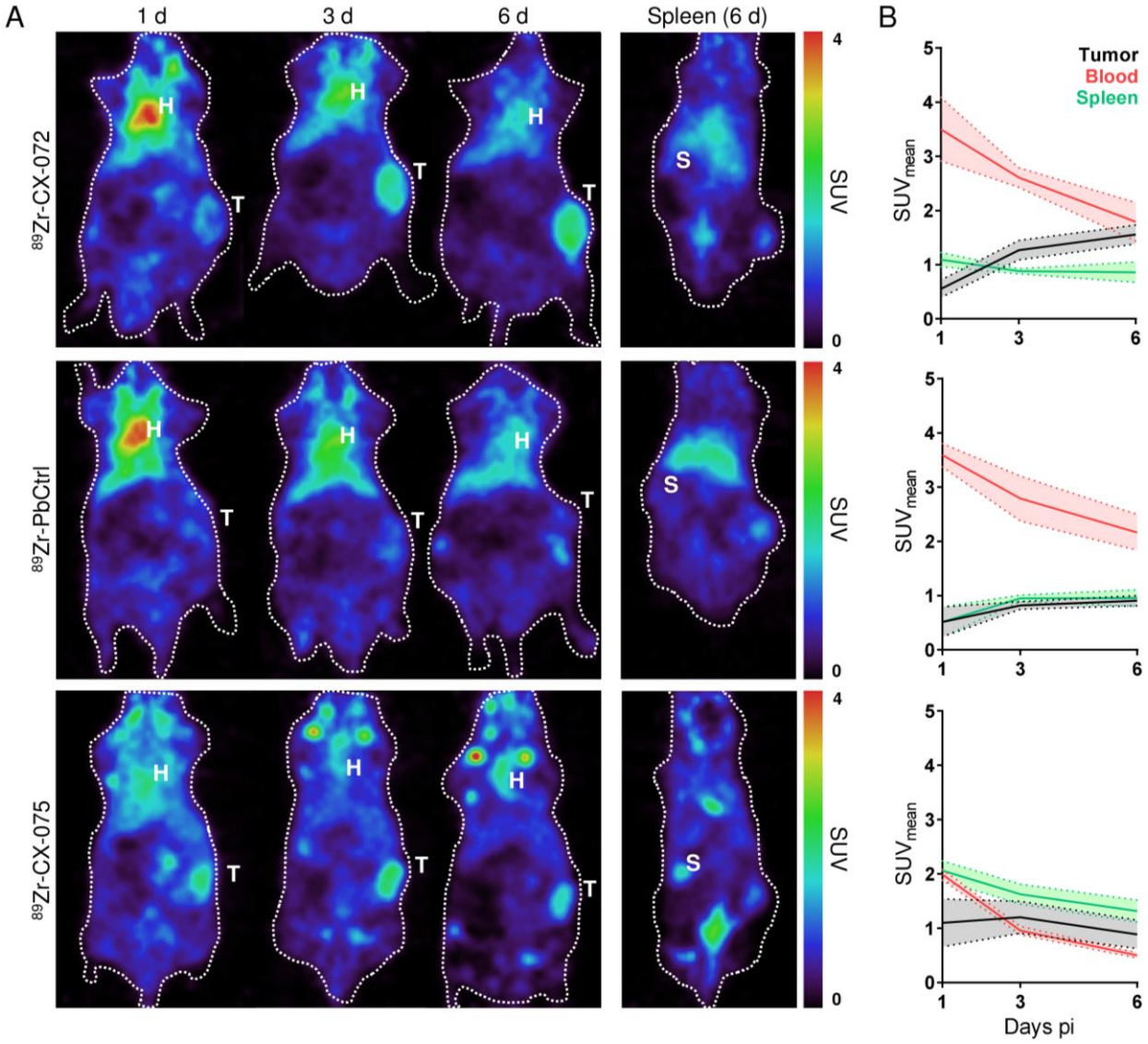

Author Manuscript Published OnlineFirst on January 17, 2020; DOI: 10.1158/1078-0432.CCR-19-3137
Author manuscripts have been peer reviewed and accepted for publication but have not yet been edited.

Figure 3

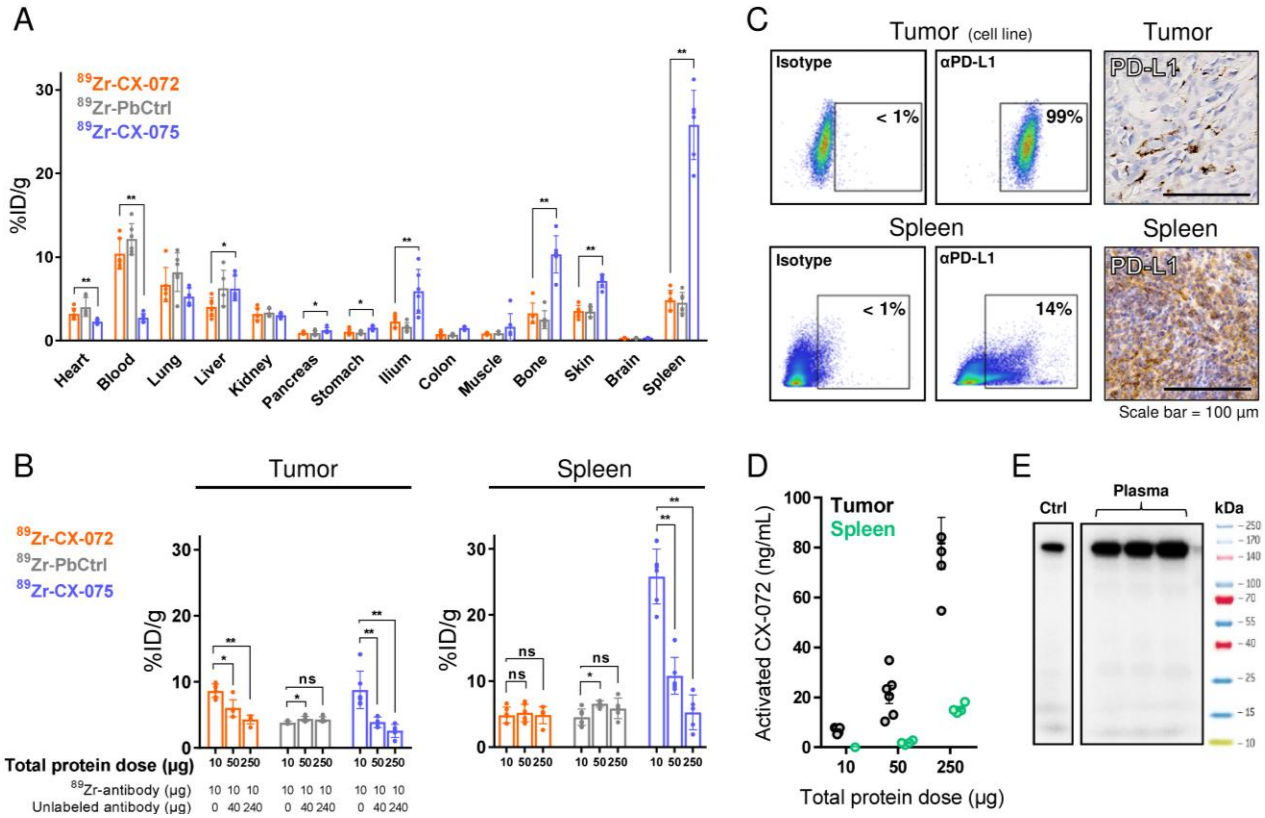

Figure 4

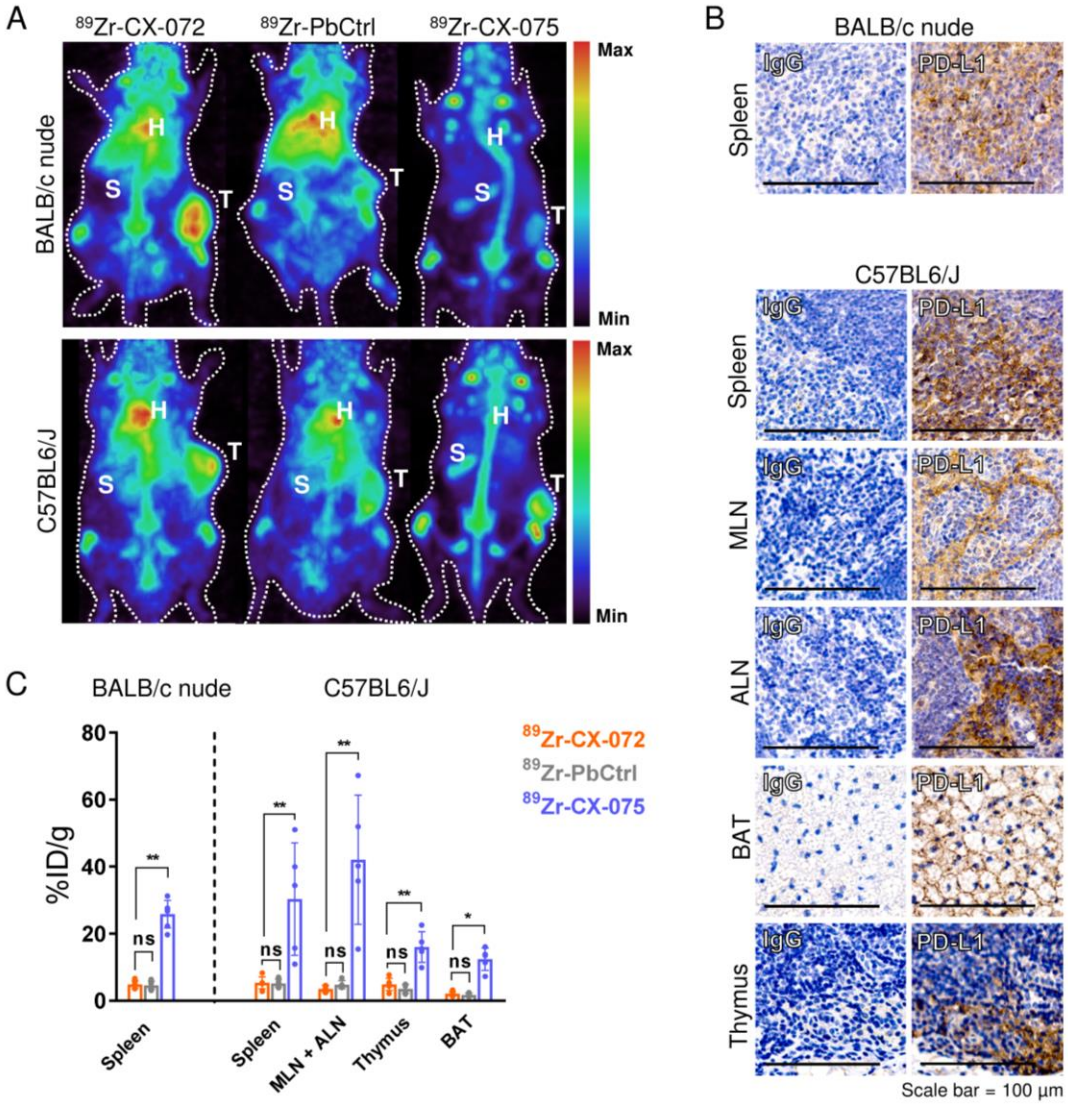

Author Manuscript Published OnlineFirst on January 17, 2020; DOI: 10.1158/1078-0432.CCR-19-3137
Author manuscripts have been peer reviewed and accepted for publication but have not yet been edited.

Figure 5

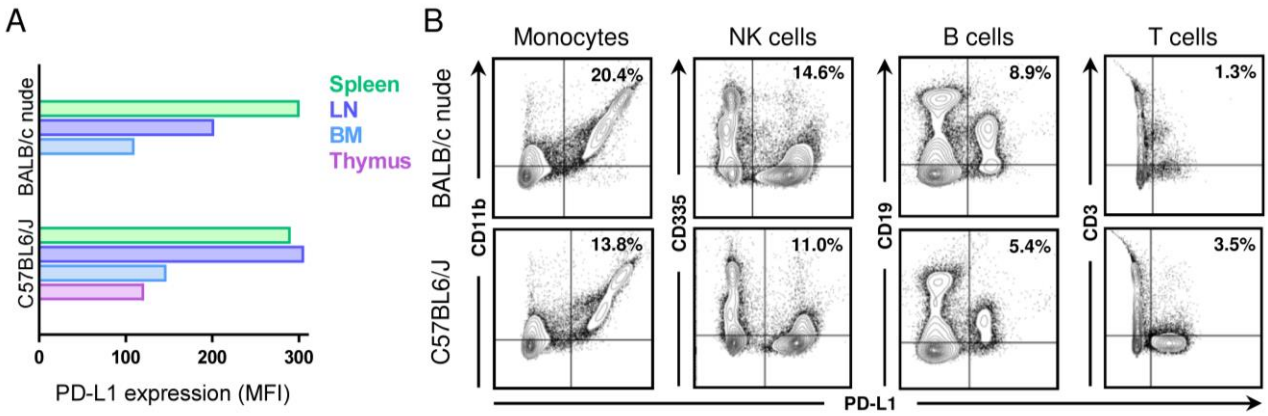

Figure 6

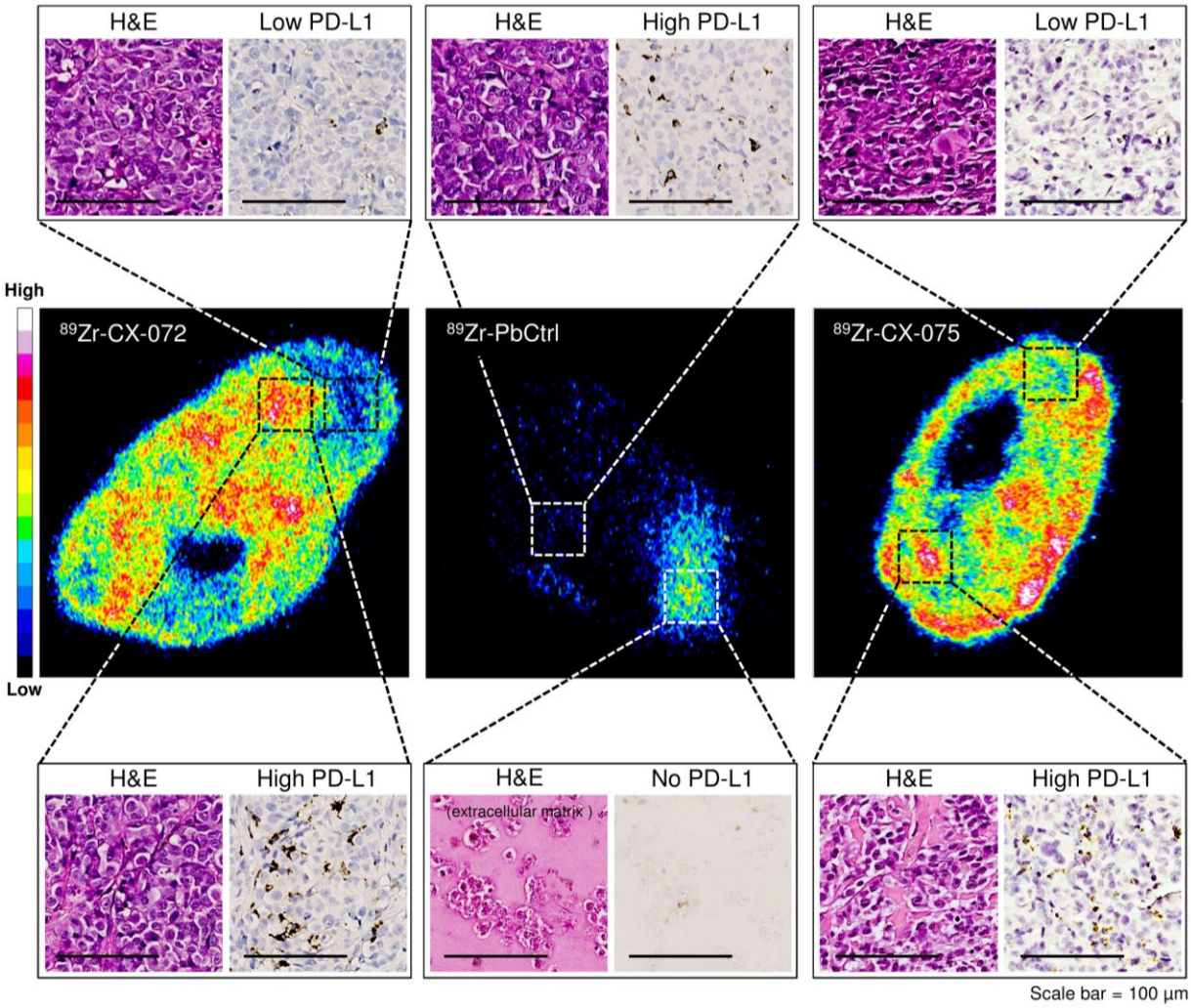

AACR American Association for Cancer Research

Clinical Cancer Research

Probody therapeutic design of 89Zr-CX-072 promotes accumulation in PD-L1 expressing tumors compared to normal murine lymphoid tissue

Danique Giesen, Linda N Broer, Marjolijn N. Lub-de Hooge, et al.

Clin Cancer Res Published OnlineFirst January 17, 2020.